CALCULATING BPM COEFFICIENTS WITH GREEN'S RECIPROCATION THEOREM

S. H. Kim
March 4, 1999

1. Introduction and Conclusion

For a highly relativistic charged beam, the Lorentz contraction compresses the electromagnetic field of the beam into the 2-D transverse plane. This results in the induced currents on the beam chamber wall having the same longitudinal intensity modulation as the charged beam. When the wavelength of the beam intensity modulation is large compared to the dimensions of the button electrodes, which are used as beam position monitors (BPMs), the calculation of the induced currents on the buttons may be simplified as a 2-D electrostatic problem. For four-button BPMs, vertical and horizontal signals are monitored from the differences in the induced charges between the top and bottom, and right and left buttons, respectively.

In this Note, the coefficients of four-button BPMs are calculated using Green's reciprocation theorem, which shows that finding induced charges on the buttons due to a charge at a beam position is equivalent to finding induced potential at a beam position due to given potentials on the buttons. In the case of finite element modeling, using the theorem significantly simplifies the calculation of BPM coefficients: the induced potential method needs only three sets of calculations for the sum, vertical, and horizontal signals, compared to one calculation for each beam position for the induced charge method. For the case of analytical expressions, two examples are given: the calculations for optimized button configurations on a small-gap chamber and the circular chamber after conformal transformations of the chamber geometry for the both cases. The BPM coefficients for the analytical results are expressed in simple formulae, which agree with the results of numerical integrals and infinite series obtained from the induced charge method.

2. Green's Reciprocation Theorem

First, we consider that a set of n charges $q_1, q_2, \ldots, q_n$ on n conductors will give rise to potentials $V_1, V_2, \ldots, V_n$ on the conductors. The potential V_m at q_m is due to all q_i except q_m. If a different set of charges $q_{p1}, q_{p2}, \ldots, q_{pn}$ gives rise to potentials $V_{p1}, V_{p2}, \ldots, V_{pn}$, then Green's reciprocation theorem [1] states that

$$\sum_{i=1}^{n} q_i V_{pi} = \sum_{i=1}^{n} q_{pi} V_i . \qquad (1)$$

Equation (1) may be applied to analyze a system of four-button BPMs as shown in the cross-section of a narrow-gap beam chamber in Fig. 1 (a). At first the beam chamber, as well as the BPM buttons, is assumed to be grounded, i.e. $V_i = 0$ (i = 1,..,4). If we place a point charge q at a beam position (x_o, y_o), then induced charges q_1, q_2, q_3, and q_4 will appear on the four buttons. (We assume that the potential at the beam position is V_s.) Now we remove the

charges at the beam position and on the buttons in order to have a new set of charges and potential distribution. This time, if we apply a potential of $+V_p$ to all four buttons (and at the same time we assume to have a charge distribution of q_{p1}, q_{p2}, q_{p3}, and q_{p4} on the four buttons), then a potential we call V_{ps} will be induced at the beam position. These two sets of charge/potential distributions are summarized in Table 1.

Table 1. Charge/Potential Distributions

	(x_o,y_o)	button 1	button 2	button 3	button 4
Charge (q_i)	q	q_1	q_2	q_3	q_4
Voltage (V_i)	V_s	0	0	0	0
Charge (q_{pi})	0	q_{p1}	q_{p2}	q_{p3}	q_{p4}
Voltage (V_{pi})	V_{ps}	V_p	V_p	V_p	V_p

Then, from the second and third rows of the table, the right side of Eq. (1) vanishes, and, from the first and fourth rows, the left side of Eq. (1) gives the relation for the sum signal

$$q\,V_{ps} + (q_1 + q_2 + q_3 + q_4)\,V_p = 0,$$

or
$$Q_s/(-q) = V_{ps}/V_p, \qquad (Q_s = q_1 + q_2 + q_3 + q_4). \tag{2}$$

We can also apply the potential V_p on the buttons in two different configurations besides the above case for all $+V_p$. By setting the upper two buttons to $+V_p$ and the lower two buttons to $-V_p$, the potential at (x_o, y_o) will be called V_{py}. Similarly, by setting the right two buttons to $+V_p$ and the left two buttons to $-V_p$, the potential at (x_o, y_o) will be called V_{px}. Then, from Eq. (1) we have

$$q\,V_{py} + (q_1 + q_2 - q_3 - q_4)\,V_p = 0,$$
$$q\,V_{px} + (q_1 - q_2 - q_3 + q_4)\,V_p = 0,$$

or
$$Q_y/(-q) = V_{py}/V_p, \qquad (Q_y = q_1 + q_2 - q_3 - q_4),$$
$$Q_x/(-q) = V_{px}/V_p, \qquad (Q_x = q_1 - q_2 - q_3 + q_4). \tag{3}$$

Equations (2) and (3) imply that Q_s, Q_y, and Q_x, corresponding to the sum, vertical, and horizontal signals for the beam position, are proportional to V_{ps}, V_{py}, and V_{px}, respectively. When the position of charge q changes, Q_s, Q_y, and Q_x change due to the redistribution of the induced charges on the buttons. This is equivalent to having different induced potentials V_{ps}, V_{py}, and V_{px} at the new beam position.

Except for a few cases of chamber geometry, derivation of analytical expressions for the induced charges on the buttons is limited. When finite element modeling has to be made for the calculation of induced charges on the buttons, one mesh geometry is required for each beam position (x_o,y_o), making it almost impossible to have a complete set of calculations for the chamber cross section, where the BPMs are located. Instead, when the induced potentials at the beam positions are chosen for the calculation by applying the Green's reciprocation theorem, the three induced potentials V_{ps}, V_{py}, and V_{px} can be calculated, after applying potentials $+V_p$ or $-V_p$ on the buttons, with only one mesh geometry, which simplifies the calculation significantly.

3. BPM Coefficients for the Optimized Configuration in a Small-Gap Beam Chamber

Figure 1 shows the conformal mapping of the inner region of a small-gap beam chamber in the z-plane into the upper half-plane of the w-plane under the transformation $w = i\exp(\pi z / 2h)$, where h is the half-gap of the chamber. We assume that the chamber width is much larger than its gap height. (A width-to height ratio larger than five gives sufficiently accurate results.) The charge $q(z_o)$ in the z-plane is now located at w_o in the w-plane. Adding an image charge $-q(\overline{w_o})$ at the complex conjugate of w_o brings the potential on the u-axis to zero. Then, from electric field $E = q/(2\pi\varepsilon_o r)$ at a distance r from a point charge $q(0)$ in a 2-D, or from a straight, infinitely long line charge in a 3-D, the electrostatic potential distribution $\Phi(x,y)$ due to $q(w_o)$ and $-q(\overline{w_o})$ in the upper half of the w-plane is calculated as

$$\Phi(x,y) = \frac{-q}{2\pi\varepsilon_o}\ln\frac{|w-w_o|}{|w-\overline{w}_o|} = \frac{-q}{4\pi\varepsilon_o}\ln\frac{\cosh p(x-x_o)-\cos p(y-y_o)}{\cosh p(x-x_o)+\cos p(y+y_o)}, \tag{4}$$

where ε_0 is the permittivity constant and $p = \pi/2h$. The same result was obtained from the infinite numbers of image charges and was used to calculate the sum, vertical, and horizontal signals [2].

For this relatively simple geometry, when a potential of $+V_p$ or $-V_p$ is applied on the buttons, the induced potentials V_{ps}, V_{py}, and V_{px} at the beam position can be calculated in the w-plane. First, assuming that the beam chamber is grounded, the induced potential at the beam position $V(x_o,y_o)$ due to potential V_p on one button, may be calculated from the Poisson's formula for the upper half-plane:

$$V(x_o,y_o) = \frac{1}{\pi}\int\frac{v_o V(\xi)d\xi}{{v_o}^2+(u_o-\xi)^2} = -\frac{V_p}{\pi}\tan^{-1}\left(\frac{u_o-\xi}{v_o}\right)\Bigg|_{\xi=u_1}^{\xi=u_2}, \tag{5}$$

where $u_o = -e^{px_o}\sin py_o$, $v_o = e^{px_o}\cos py_o$, u_1 and u_2 are the button locations corresponding to x_1 and x_2 in Fig. 1 (a). Then, for four buttons located symmetrically with respect to the x- and y-axes, V_{ps}, V_{py}, and V_{px} are calculated from Eq. (5):

$$V_{ps}(x_o,y_o) = \frac{V_p}{\pi}\left[\tan^{-1}\left\{\frac{\sinh p(x-x_o)}{\cos py_o}\right\}+\tan^{-1}\left\{\frac{\sinh p(x+x_o)}{\cos py_o}\right\}\right]_{x=x_1}^{x=x_2}, \tag{6}$$

$$V_{py}(x_o,y_o) = \frac{V_p}{\pi}\left[\tan^{-1}\left\{\frac{e^{2p(x-x_o)}+\cos 2py_o}{\sin 2py_o}\right\}-\tan^{-1}\left\{\frac{e^{-2p(x+x_o)}+\cos 2py_o}{\sin 2py_o}\right\}\right]_{x_1}^{x_2}, \tag{7}$$

and

$$V_{px}(x_o,y_o) = \frac{V_p}{\pi}\left[\tan^{-1}\left\{\frac{\sinh p(x-x_o)}{\cos py_o}\right\}-\tan^{-1}\left\{\frac{\sinh p(x+x_o)}{\cos py_o}\right\}\right]_{x_1}^{x_2}. \tag{8}$$

When V_p is replaced with (-q), Eqs. (6) - (8) are indeed identical to the integral forms of Q_s, Q_y, and Q_x in reference [2]. By substituting the button positions (x_1 and x_2) and the half-gap height h ($p = \pi/2h$) in Eqs. (6) - (8), sum, vertical, and horizontal signals and BPM coefficients can be calculated directly from V_{py}/V_{ps} and V_{px}/V_{ps}.

Figure 2 shows 3-D plots of the sum, vertical, and horizontal signals as well as their normalized signals to the sum signal in the plane of normalized beam position to half-gap of the chamber (xo = x_o/h, yo = y_o/h) for V_p = 1.0. The 3-D plots are calculated for the case of x_1 = 0 and x_2 = 2h (button diameter of 2h), which is the optimized BPM configuration in a small-gap beam chamber [2]. The sum and vertical signals start to decrease in |xo| > 1.5. For |xo| < 2, the normalized vertical signal has excellent linearity with respect to the vertical beam position. The horizontal and its normalized signals, on the other hand, are highly nonlinear compared to the vertical one, even for |xo| < 0.5.

In Fig. 3, normalized signals are plotted at selected values of xo and yo. For |xo| < 2, the linearity for the vertical signal is shown again to be very close to the chamber wall in the vertical direction. The horizontal signal becomes relatively insensitive to the beam position for |xo| > 1. Polynomial coefficients of the BPM and their inversions to the third and fifth orders are listed in Table 2. The R value in the table is defined as the square root of

$$R^2 = 1 - \sum (y_i - y_o)^2 / \{\sum y_i^{\,2} - (\sum y_i)^2 / n\},$$

where y_i is the actual input data for the plot, y_o is the estimated values using the coefficients in the table, and n is the number of data points. R ranges from 0 to 1. If R is 1, there is no difference between the actual data and estimated ones using the polynomial coefficients.

4. BPM Coefficients in a Circular Beam Chamber

Four-button BPMs in a circular beam chamber of radius a in the z-plane (Fig. 4(a)) are mapped into the w-plane (Fig. 4(b)) under the transformation $w = u + iv = i(1+z)/(1-z)$, where z is normalized to the chamber radius. The buttons are located symmetrically with respect to the x- and y-axes of the chamber. The induced potential $V(x_o,y_o)$ due to potential V_p on button (1), located in the first quadrant, can be calculated from Eq. (5) with

$$\begin{aligned} &u_o = -2y_o/[(1-x_o)^2 + y_o^{\,2}], \quad v_o = (1-x_o^{\,2} - y_o^{\,2})/[(1-x_o)^2 + y_o^{\,2}], \\ &\xi(\theta) = -\sin\theta/(1-\cos\theta), \\ &\theta_1 = \theta_p - \Delta\theta/2, \quad \theta_2 = \theta_p + \Delta\theta/2, \quad \Delta\theta = \theta_2 - \theta_1. \end{aligned} \tag{9}$$

Then, by adding up the induced potential from the four buttons, the potential for the sum signal can be calculated from

$$\begin{aligned} V_{ps}(x_o, y_o) = -\frac{V_p}{\pi}\Bigg[&\tan^{-1}\{\frac{u_o - \xi(\theta)}{v_o}\}\Big|_{\theta 1}^{\theta 2} + \tan^{-1}\{\frac{u_o - \xi(\theta)}{v_o}\}\Big|_{\pi-\theta 2}^{\pi-\theta 1} \\ &+ \tan^{-1}\{\frac{u_o - \xi(\theta)}{v_o}\}\Big|_{\pi+\theta 1}^{\pi+\theta 2} + \tan^{-1}\{\frac{u_o - \xi(\theta)}{v_o}\}\Big|_{2\pi-\theta 2}^{2\pi-\theta 1}\Bigg]. \end{aligned} \tag{10}$$

The induced potentials, $V_{py}(x_o,y_o)$ and $V_{px}(x_o,y_o)$, for the vertical and horizontal signals can be obtained with minus signs in the third and fourth terms, and with minus signs in the second and third terms, respectively, in Eq. (10). The induced charges associated with the sum, vertical, and horizontal signals for four-button BPMs in a circular beam chamber of radius a, shown in Fig. 4(a), are given by [3]

$$Q_s = -\rho_k \frac{4\Delta\theta}{2\pi}[1+\sum_{n=1}^{\infty}\{1+(-1)^n\}(\frac{r_o}{a})^n \cos n\theta_p \cos n\theta_o(\frac{\sin n\Delta\theta/2}{n\Delta\theta/2})],$$

$$Q_y = -\rho_k \frac{4\Delta\theta}{2\pi}\sum_{n=1}^{\infty}\{1-(-1)^n\}(\frac{r_o}{a})^n \sin n\theta_p \sin n\theta_o(\frac{\sin n\Delta\theta/2}{n\Delta\theta/2}),$$

$$Q_x = -\rho_k \frac{4\Delta\theta}{2\pi}\sum_{n=1}^{\infty}\{1-(-1)^n\}(\frac{r_o}{a})^n \cos n\theta_p \cos n\theta_o(\frac{\sin n\Delta\theta/2}{n\Delta\theta/2}). \quad (11)$$

By replacing $-\rho_k$ with V_p, Eq. (11) should give the identical results with Eq. (10), $V_{py}(x_o,y_o)$, and $V_{px}(x_o,y_o)$. Indeed, for a = 35 mm, $\theta_p = \pi/4$, $\theta_1 = 0.5239$ rad, and $\theta_2 = 1.0469$ rad, ($\Delta\theta/2 = 0.2615$ rad) one can show numerically that, with n = 10 terms for $r_o/a = 0.4$ and n = 75 terms for $r_o/a = 0.9$, the two methods agree to within 5×10^{-6}.

Figure 5 shows the induced potentials associated with the sum and normalized vertical signals as functions of yo = y_o/a at four selected values of xo = x_o/a for the above chamber radius and angular positions of the buttons. (For $\theta_p = \pi/4$, V_{py} and V_{px} should give the same value.) Polynomial coefficients of the BPM and their inversions to the third order for |yo| < 0.5 are listed in Table 3.

From the induced potentials, 3-D plots in the plane of ro = r_o/a and th = angle (rad) for the sum, vertical, and normalized vertical signals with V_p.=1.0 are shown in Fig. 6. The buttons occupy approximately 1/3 of the chamber circumference, so that V_{ps} near ro = 0 is 0.33. When the beam positions are close to those of the buttons, both V_{ps} and V_{py} are much larger than 0.5; those parts are not shown in Fig. 6(a). However, as shown in Fig. 6(b), the normalized values V_{py}/V_{ps} vary rather smoothly even near the buttons. The variations of V_{ps} and V_{py}/V_{ps} at th = $\pi/2$ rad along the radius in Fig. 6 correspond to the curves for xo = 0 in Fig. 5.

When the four buttons are located at the top (T), bottom (B), right (R), and left (L) of the circular chamber in Fig. 4(a) instead of at $\theta_p = \pi/4$, two sets of buttons, T and B, and R and L, can be used for vertical and horizontal BPMs, respectively. The sum signal for the vertical BPM is given by

$$V_{T+B}(x_o, y_o) = -\frac{V_p}{\pi}\left[\tan^{-1}\{\frac{u_o-\xi(\theta)}{v_o}\}\Big|_{\pi/2-\Delta\theta/2}^{\pi/2+\Delta\theta/2} + \tan^{-1}\{\frac{u_o-\xi(\theta)}{v_o}\}\Big|_{3\pi/2-\Delta\theta/2}^{3\pi/2+\Delta\theta/2}\right], \quad (12)$$

where parameters u_o, v_o, and $\xi(\theta)$ are listed in Eq. (9). The vertical signal, $V_{T-B}(x_o,y_o)$, is calculated with a minus sign in the second term in Eq. (12). Horizontal signals can be calculated by replacing $\pi/2$ and $3\pi/2$ with zero and π in the above equation.

The sum and normalized signals are plotted in Fig. 7 with $\Delta\theta/2 = 0.2615$ rad. For $|yo| < 0.5$, the signal magnitudes with two buttons are approximately one half of those with four buttons, as seen from Fig. 5. With two buttons, however, the dependence of the normalized vertical signal to the horizontal beam position is much smaller compared to the four buttons in Fig. 5(b). Polynomial coefficients of the BPM and their inversions to the third order for $|yo| < 0.5$ are listed in Table 4. In Fig. 8 the sum, vertical, and normalized vertical signals are plotted in the plane of ro = r_o/a and th = angle (rad). The normalized signal at th = $\pi/2$ corresponds to Fig. 7(b) at xo = 0.

Acknowledgements

The author appreciates G. Decker and L. Emery for their numerous suggestions for this work.

References

[1] W. K. H. Panofsky and M. Phillips, *Classical Electricity and Magnetism*, Addison-Wesley (1955), p. 38.
[2] S. H. Kim, "Optimization of Four-Button BPM Configuration for Small-Gap Beam Chambers," *Proc. of the Beam Instrumentation Workshop,* AIP Conf. Proc. **451**, p. 310 (1998).
[3] S. H. Kim, "Four-Button BPM Coefficients in Cylindrical and Elliptic Beam Chambers," LS Note LS-274 (1999).

Table 2. Four-button BPM coefficients for optimized configuration ($x_1 = 0$ and $x_2 = 2h$) of a narrow beam chamber. (a) and (b) are coefficients for normalized vertical signals and their inversions for $|yo| < 0.75$ to the third order at selected values of xo where $xo = x_o/h$ and $yo = y_o/h$. (c) and (e) are coefficients for normalized horizontal signals and their inversions for $|xo| < 0.5$ to the fifth order at four selected values of yo; (d) and (f) are to the third order.

(a) $Y = M_1\, yo + M_3\, yo^3$, ($Y = V_{py}/V_{ps}$): Normalized vertical signal						
	xo = 0	**xo = 0.5**	**xo = 1.0**	**xo = 1.5**	**xo = 2.0**	**xo = 2.5**
M_1	1.0531	1.0671	1.1087	1.1456	1.0023	0.63811
M_3	-0.05919	-0.07432	-0.11671	-0.13112	-0.00257	-0.15317
R	1	1	1	1	1	1
(b) $yo = m_1\, Y + m_3\, Y^3$, (Inverted polynomial coefficients)						
m_1	0.94886	0.93604	0.89952	0.87005	0.99767	1.5424
m_3	0.053523	0.065415	0.094456	0.094678	0.002561	1.4707
R	1	1	1	1	1	0.99997
(c) $X = N_1 xo + N_3\, xo^3 + N_5\, xo^5$, ($X = V_{px}/V_{ps}$): Normalized horizontal signal)						
	yo=0	**yo=0.25**	**yo=0.5**	**yo=0.75**		
N_1	0.96141	1.0438	1.3423	2.0845		
N_3	-0.34894	-0.46193	-0.94616	-2.5025		
N_5	0.099612	0.15388	0.40996	1.3483		
R	1	1	0.99996	0.99911		
(d) $X = N_1 xo + N_3\, xo^3$						
N_1	0.96343	1.0492	1.3728	2.284		
N_3	-0.33966	-0.46131	-1.0393	-3.4263		
R	1	1	0.99998	0.99938		
(e) $xo = n_1\, X + n_3\, X^3 + n_5\, X^5$, (Inverted polynomial coefficients)						
n_1	1.0443	0.95933	0.73633	0.4899		
n_3	0.31738	0.31084	0.17632	-0.53407		
n_5	0.77616	0.80171	0.97583	1.6125		
R	1	1	0.99999	0.99981		
(f) $xo = n_1\, X + n_3\, X^3$						
n_1	1.030	0.94127	0.69701	0.32245		
n_3	0.54812	0.5761	0.61178	0.61998		
R	1	1	0.99999	0.99971		

Table 3. Four-button BPM coefficients for normalized vertical signals and their inversions in the circular chamber of Fig. 4(a) for |yo| < 0.5 at four selected values of xo, where xo = x_o/a, yo = y_o/a, and a is the chamber radius.

(a) $Y = M_1\, yo + M_3\, yo^3$, ($Y = V_{py}/V_{ps}$)				
	xo=0	**xo=0.2**	**xo=0.4**	**xo=0.6**
M1	1.3835	1.5297	1.9125	2.3816
M3	-0.98581	-1.1066	-1.609	-2.5389
R	1	1	0.99999	0.99999
(b) $yo = m_1\, Y + m_3\, Y^3$, (Inverted polynomial coefficients)				
	xo=0	**xo=0.2**	**xo=0.4**	**xo=0.6**
m_1	0.69876	0.63119	0.49711	0.3834
m_3	0.51833	0.39346	0.26299	0.21581
R	0.99998	0.99998	0.99996	0.99981

Table 4. Two-button BPM coefficients for normalized vertical signals and their inversions in the circular chamber for |yo| < 0.5 at four selected values of xo where xo = x_o/a, yo = y_o/a, and a is the chamber radius. The two buttons are located at the top ($\theta_p = \pi/2$) and bottom ($\theta_p = 3\pi/2$) of Fig. 4(a).

(a) $Y = M_1\, yo + M_3\, yo^3$, ($Y = V_{py}/V_{ps}$)				
	xo=0	**xo=0.2**	**xo=0.4**	**xo=0.6**
M1	1.9538	1.8925	1.7257	1.4965
M3	-1.5189	-1.4066	-1.1531	-0.8810
R	0.99999	0.99999	1	1
(b) $yo = m_1\, Y + m_3\, Y^3$, (Inverted polynomial coefficients)				
	xo=0	**xo=0.2**	**xo=0.4**	**xo=0.6**
m_1	0.49094	0.50899	0.56285	0.65388
m_3	0.21394	0.21763	0.23982	0.30008
R	0.99997	0.99998	0.99999	0.99999

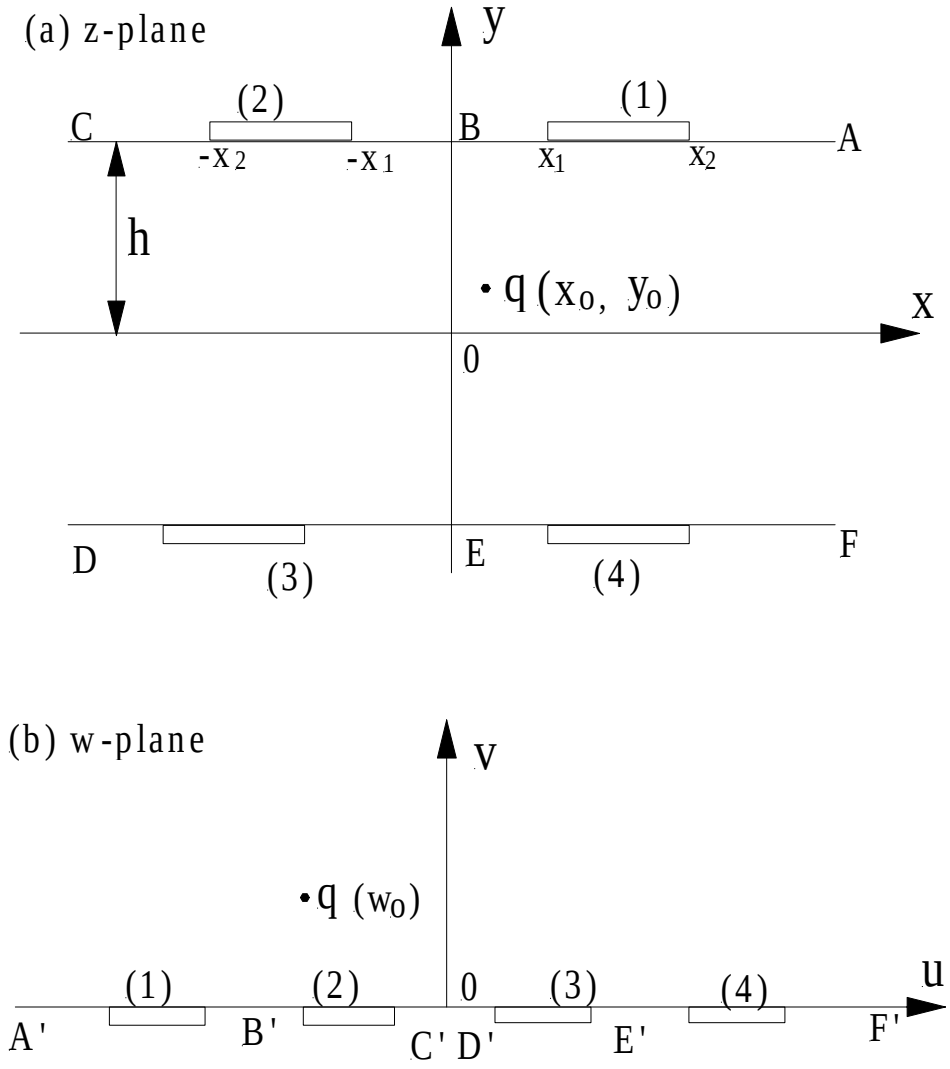

Fig. 1. Conformal mapping of a small-gap beam chamber with a relatively large chamber width-to-height aspect ratio from (a) z-plane to (b) w-plane using a transformation of $w = i \exp(\pi z/2h)$, where h is the half-gap of the chamber. The buttons are located symmetrically with respect to the x- and y-axes in the z-plane.

(a) Sum (V_{ps})

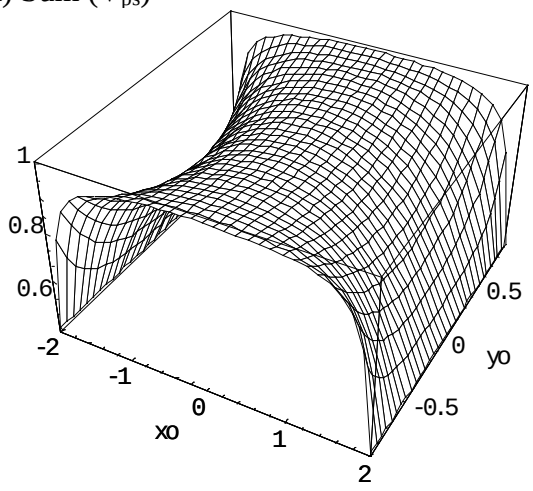

(b) Vert (V_{py})

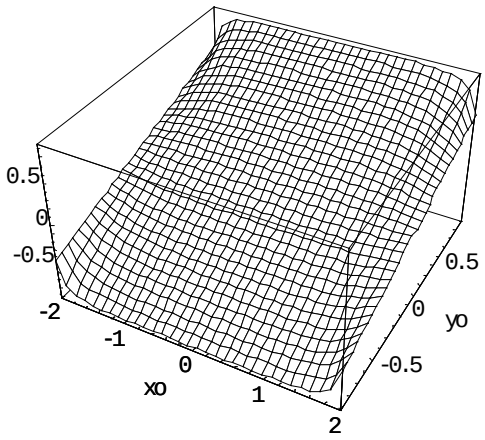

Vert/Sum (V_{py}/V_{ps})

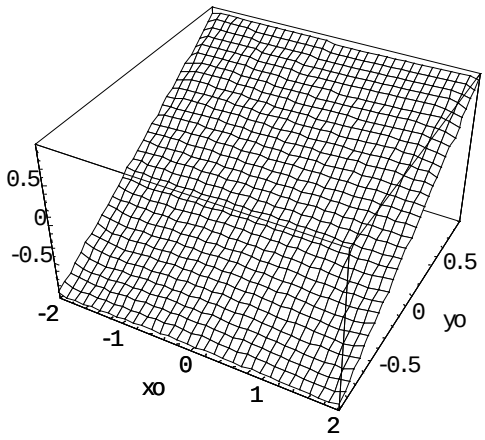

(c) Horz (V_{px})

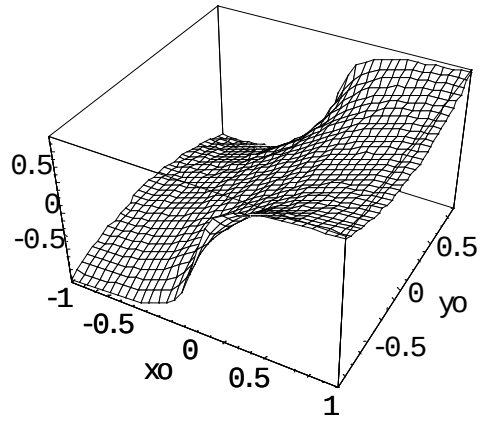

Horz/Sum (V_{px}/V_{ps})

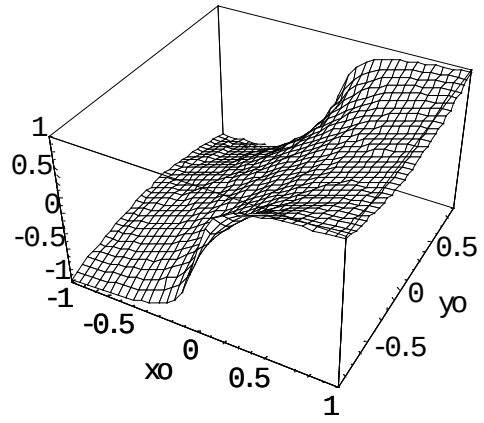

Fig. 2. 3-D plots for (a) sum (V_{ps}), (b) vertical (V_{py}) and normalized vertical (V_{py}/V_{ps}), and (c) horizontal (V_{px}) and normalized horizontal (V_{px}/V_{ps}) signals in the plane of xo = x_o/h and yo = y_o/h for the optimized configuration in a small-gap beam chamber.

(a)

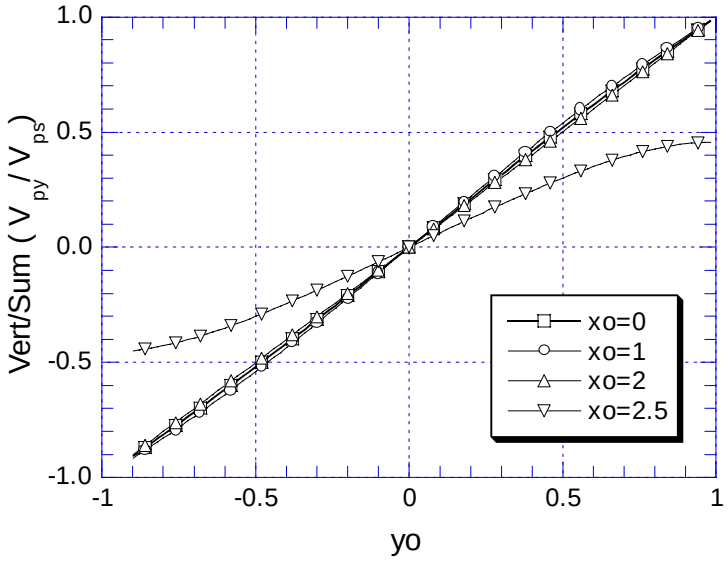

(b)

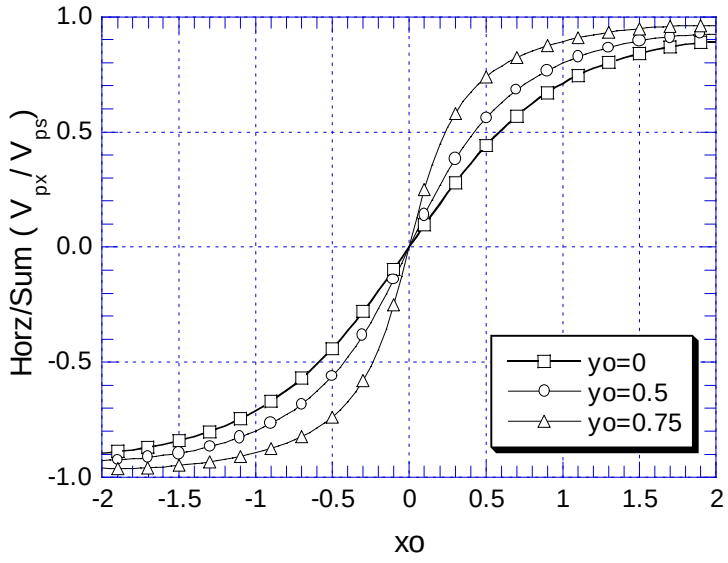

Fig. 3. (a) Normalized vertical (V_{py}/V_{ps}) and (b) normalized horizontal (V_{px}/V_{ps}) signals as functions of beam positions xo = x_o/h and yo = y_o/h for the optimized configuration in a small-gap beam chamber.

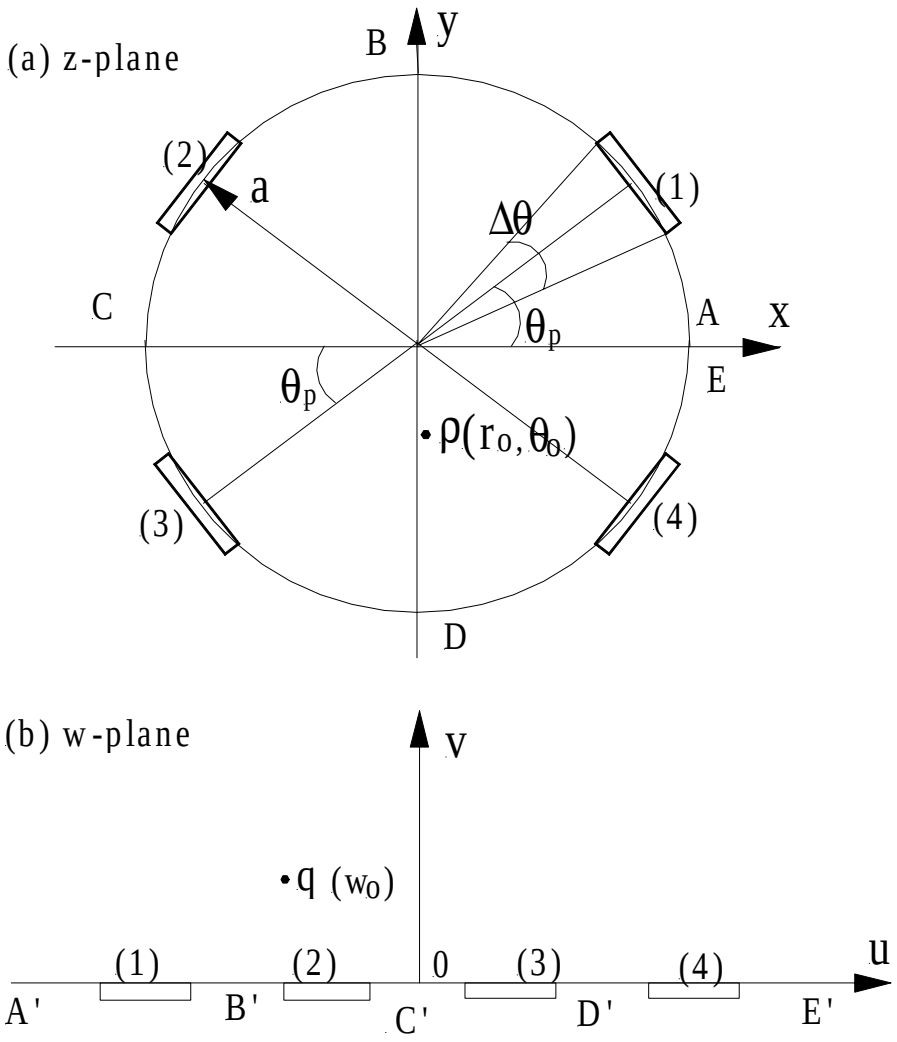

Fig. 4. Conformal mapping of a circular chamber from (a) z-plane to (b) w-plane using a transformation of $w = u + iv = i(1+z)/(1-z)$, where z is normalized to the chamber radius a. The buttons are located symmetrically with respect to the x- and y-axes in the z-plane.

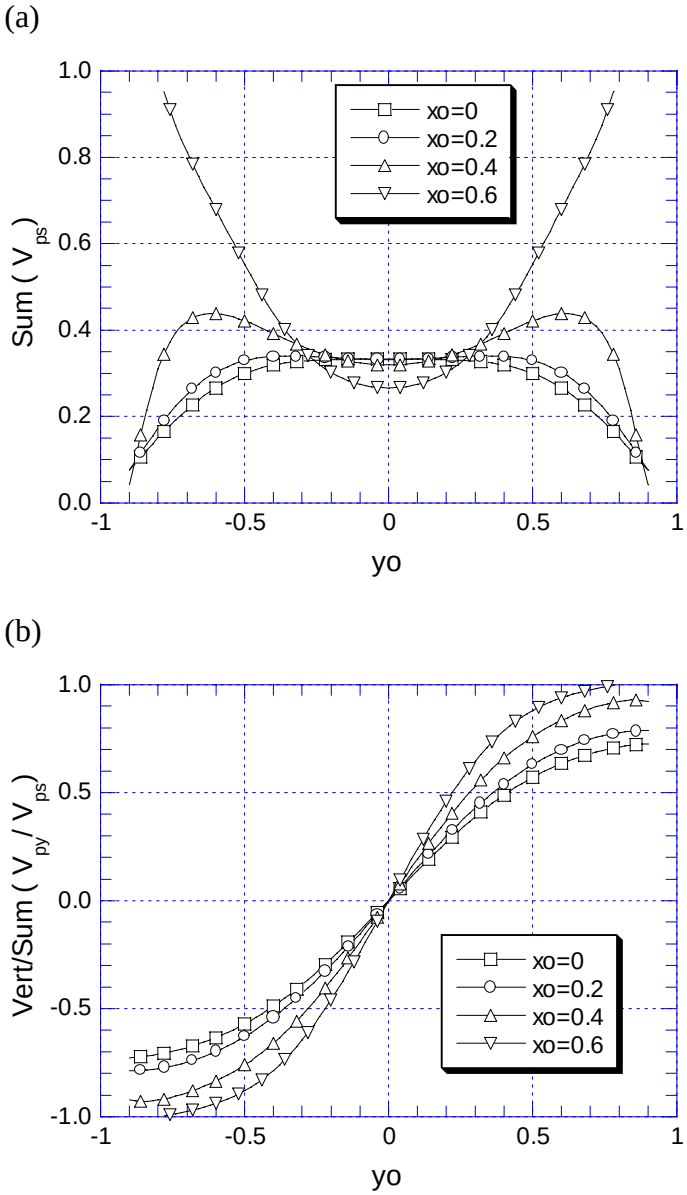

Fig. 5. (a) Sum (V_{ps}) and (b) normalized vertical (V_{py}/V_{ps}) signals as functions of beam position yo = y_o/a at selected values of xo = x_o/a for four-button BPMs in the circular beam chamber (Fig. 4) with parameters of a = 35 mm, $\theta_p = \pi/4$, $\theta_1 = 0.5239$ rad, and $\theta_2 = 1.0469$ rad.

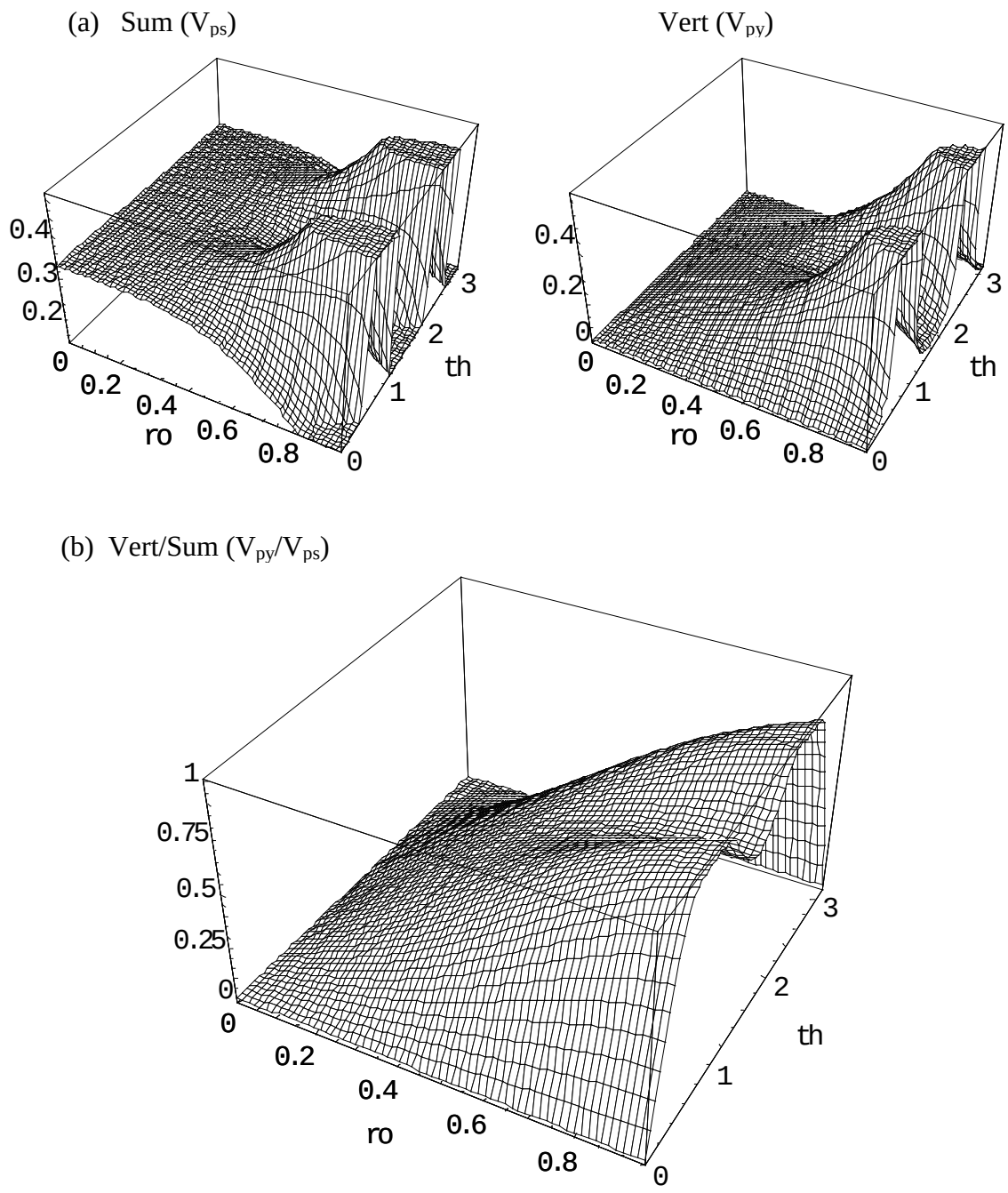

Fig. 6. 3-D plots for (a) sum (V_{ps}), vertical (V_{py}) and (b) normalized vertical (V_{py}/V_{ps}) signals in the plane of ro = r_o/a and th = angle (rad) for four-button BPMs in the circular beam chamber (Fig. 4) with parameters of a = 35 mm, $\theta_p = \pi/4$, $\theta_1 = 0.5239$ rad, and $\theta_2 = 1.0469$ rad. When the beam position is near the buttons, the sum and vertical signal become large, as shown for V_{ps} at xo = 0.6 in Fig. 5(a), and were cut at 0.5. The values of V_{py}/V_{ps} along ro at th = $\pi/2$ rad correspond to Fig. 5(b) at xo=0.

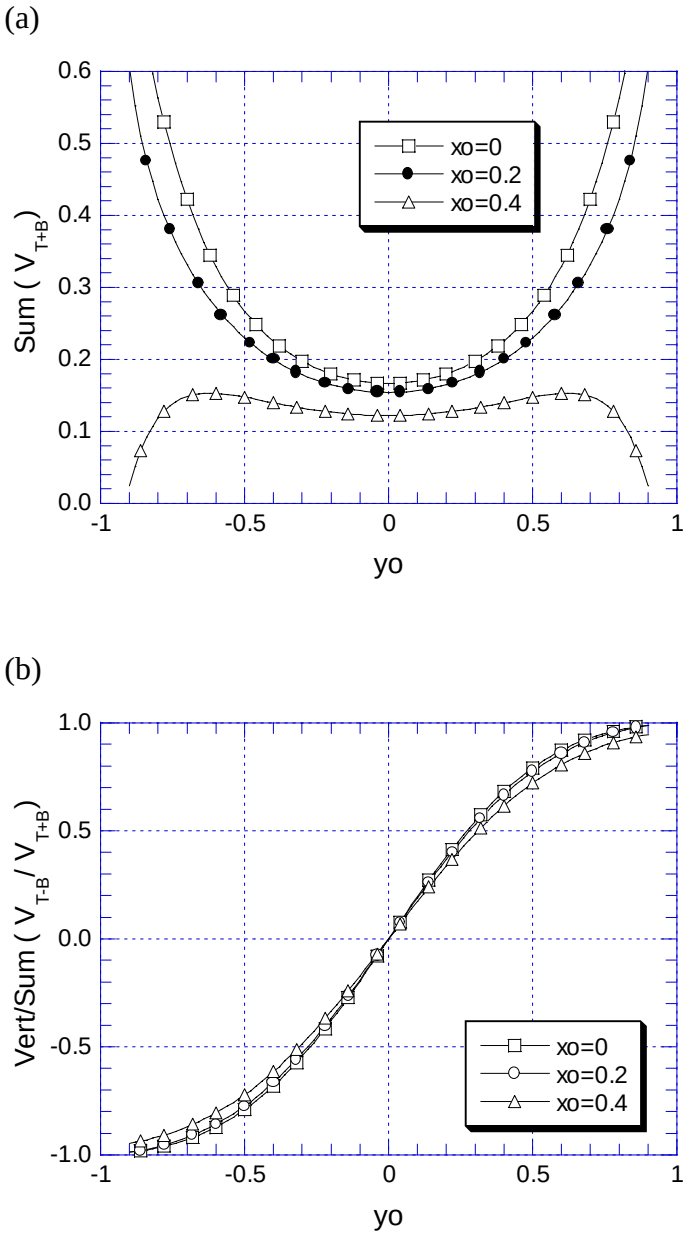

Fig. 7. (a) Sum (V_{T+B}) and (b) normalized vertical (V_{T-B}/V_{T+B}) signals as functions of beam position yo = y_o/a at selected values of xo = x_o/a for two-button BPMs located at the top ($\theta_p = \pi/2$) and bottom ($\theta_p = 3\pi/2$) of the circular beam chamber in Fig. 4 with parameters of a = 35 mm and $\Delta\theta/2 = 0.2615$ rad.

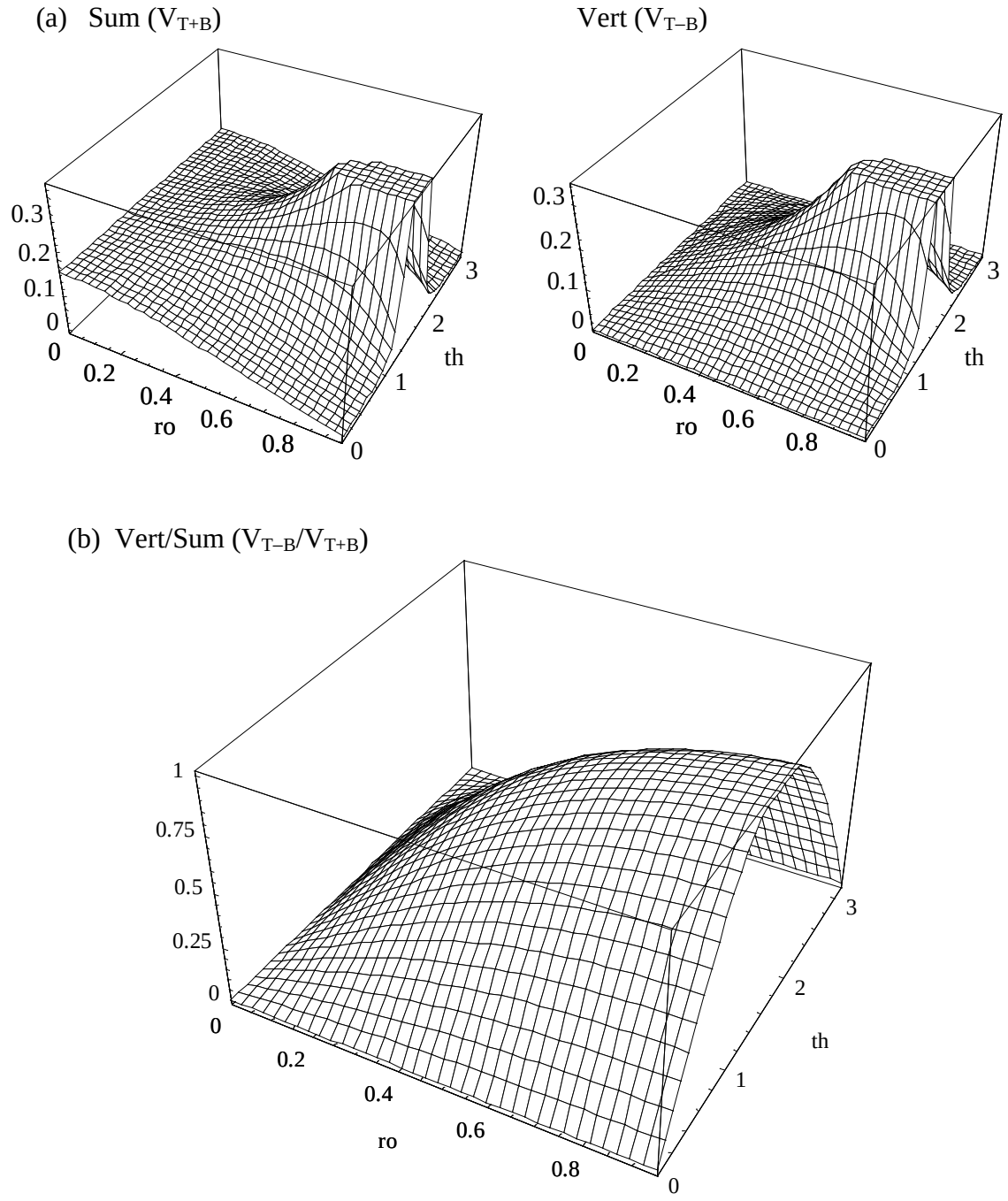

Fig. 8. 3-D plots for (a) sum (V_{T+B}), vertical (V_{T-B}) and (b) normalized vertical (V_{T-B}/V_{T+B}) signals in the plane of ro = r_o/a and th = angle (rad) for two-button BPMs located at the top and bottom of the circular beam chamber in Fig. 4 with parameters of a = 35 mm and $\Delta\theta/2$ = 0.2615 rad. When the beam position is near the buttons, the sum and vertical signal become large, as shown for V_{T+B} at xo = 0.2 and 0.4 in Fig. 7(a), and were cut at 0.35. The values of V_{T-B}/V_{T+B} along ro at th = $\pi/2$ rad correspond to Fig. 7(b) at xo=0.